High Resolution Broad-Band Spectroscopy in the NIR Using the TripleSpec Externally Dispersed Interferometer at the Hale Telescope

David J. Erskine[a], J. Edelstein[b], M. Sirk[b], E. Wishnow[b], Y. Ishikawa[b], E. McDonald[b], W. V. Shourt[b]

[a]Lawrence Livermore Nat. Lab., Livermore, CA
[b]Space Sciences Lab., Univ. of Calif., Berkeley, CA

ABSTRACT

High resolution broad-band spectroscopy at near-infrared wavelengths has been performed using externally dispersed interferometry (EDI) at the Hale telescope at Mt. Palomar. The EDI technique uses a field-widened Michelson interferometer in series with a dispersive spectrograph, and is able to recover a spectrum with a resolution 4 to 10 times higher than the existing grating spectrograph. This method increases the resolution well beyond the classical limits enforced by the slit width and the detector pixel Nyquist limit and, in principle, decreases the effect of pupil variation on the instrument line-shape function. The EDI technique permits arbitrarily higher resolution measurements using the higher throughput, lower weight, size, and expense of a lower resolution spectrograph. Observations of many stars were performed with the TEDI interferometer mounted within the central hole of the 200 inch primary mirror. Light from the interferometer was then dispersed by the TripleSpec near-infrared echelle spectrograph. Continuous spectra between 950 and 2450 nm with a resolution as high as ∼27,000 were recovered from data taken with TripleSpec at a native resolution of ∼2,700. Aspects of data analysis for interferometric spectral reconstruction are described. This technique has applications in improving measurements of high-resolution stellar template spectra, critical for precision Doppler velocimetry using conventional spectroscopic methods. A new interferometer to be applied for this purpose at visible wavelengths is under construction.

Keywords: High resolution spectroscopy, Externally Dispersed Interferometry, Dispersed Fixed Delay Interferometry, Resolution Boosting, Doppler radial velocimetry, Fourier Transform Spectroscopy, Exoplanets

1. INTRODUCTION

Wide bandwidth high resolution spectroscopy is one of the most valuable diagnostic tools for astronomy, from Doppler radial velocimetry in the search for exoplanets, to studying the characteristics of stars through the size, breadth and position of spectral features. A wide bandwidth is needed in radial velocimetry to collect as many photons as possible to reduce velocity noise. Wide bandwidth is desired for analysis of species population because the characteristic wavelengths are often distributed over a wide band. However it is difficult to achieve both wide bandwidth and high spectral resolution, since this requires not only a large and expensive instrument, but also a detector with many pixels. This is especially so for infrared wavelengths since the spectrograph size scales with resolving power times wavelength.

A novel technique called externally dispersed interferometry[1] (EDI) can dramatically reduce the necessary size of spectrographs for Doppler radial velocimetry[1–7] and high resolution spectroscopy.[8–12] We have demonstrated EDI in both applications, in the near-infrared at the Hale 5-m telescope at Mt. Palomar Observatory. Other workers have adopted the EDI method from our laboratories and demonstrated a Doppler planet detection.[5] This report focuses on the high resolution spectroscopy application.

Author information:
D.E.: erskine1@llnl.gov, J.E.: jerrye@ssl.berkeley.edu

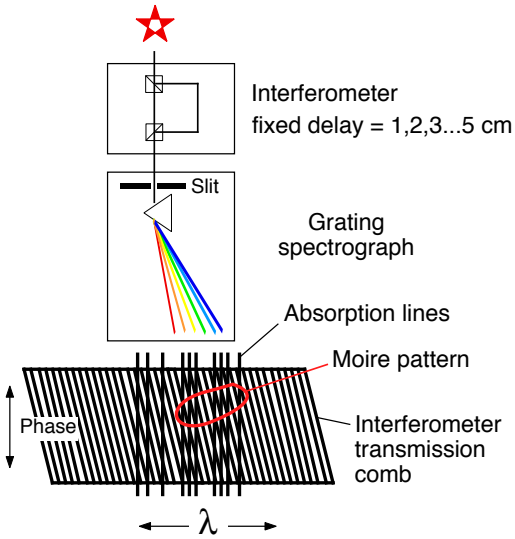

Figure 1. Externally Dispersed Interferometer (EDI) scheme. The sinusoidal transmission comb of the interferometer multiplies the stellar spectrum yielding a moiré pattern. This manifests high resolution spectral information (high feature frequency) heterodyned down to broad and detectable features (low feature frequency). The interferometer delay (optical path difference) is chosen from several fixed values, typically 1 to 5 cm, to sense different feature frequency regions. The overall moiré phase shifts in proportion to target Doppler velocity, and is the subject of other reports.[1,2] The *shape* of moiré pattern encodes the shape of the high resolution spectrum. The topic of this paper is to reversing the heterodyning process and deducing the original spectrum from a series of moiré patterns measured at different delays.

The EDI technique uses a field-widened Michelson interferometer in series with a dispersive spectrograph to heterodyne unresolvable narrow features to a detectable low frequency moiré pattern (Fig. 1). A series of phase-stepped exposures are taken with a sequence of one to a few fixed delay values, which map out delay-space up to a maximum value τ_{max} of a few cm (4.5 cm). After Fourier processing to shift the frequencies to their original value, a spectrum with a resolution 4 to 10 times higher than the existing grating spectrograph has been recovered. The resolving power is set by the number of wavelengths λ which fit inside the maximum delay (τ_{max}/λ). In contrast with a dispersive spectrograph, it is now independent of the slit width, focal blur, pixel Nyquist limitations, and grating dispersion.[8,10,11]

1.1 Enabler and Enhancer

Figure 2 shows an example of a 10x resolution boost, achieving 27,000 resolution (red curve) from a native TripleSpec[13] spectrograph (green dashed curve) having only 2,700 resolution. None of the individual absorption lines are resolved by the native spectrograph in that Figure. Yet these lines contain all the scientific information we seek about the star. The EDI reconstructed spectrum fully resolves all these lines, **enabling the inexpensive, high throughput, wide bandwidth but low resolution spectrograph to become a powerful high resolution instrument**.

1.2 Interferometer Component Performs High Resolution Duties

It is the interferometer component, rather than the disperser, which performs the fine wavelength measurement. The interferometer is "crossed" with the disperser. The former is like the vernier which performs the fine measurement, the latter is like the coarse tuner which merely separates the light into channels which have enhanced fringe visibility because the bandwidth of individual channels is narrowed. Since the interferometer component is small (∼50 cm), it is much easier to put in a stable environment than a stand-alone disperser, which for a 50,000 resolution can be of several meters size. The interferometer has only 3 degrees of freedom compared to the dozen or more that effect the point spread function (PSF) of a typical echelle grating spectrograph. This makes the instrument lineshape much more robust to environmental insults (see simulations in Fig. 10 of Ref. 8).

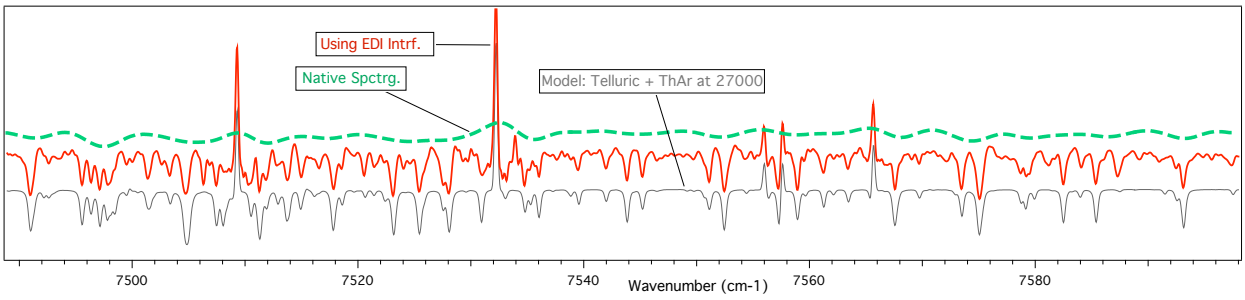

Figure 2. Demonstration of a 10-fold resolution boost observing telluric features mixed into spectrum of star κ CrB along with ThAr calibration lamp emission lines. The green dashed (top) curve is the "ordinary" spectrum measured without the interference, having native resolution 2,700. It cannot resolve any of the telluric features. The red (middle) curve is the EDI (TEDI) reconstructed spectrum measured with 7 contiguous delays, up to 3 cm, and equalized to a Gaussian resolution of 27,000. The gray (bottom) curve is a model of telluric[14] and ThAr[15] features blurred to resolution of 27,000, showing excellent agreement with EDI reconstructed data. Resolution boosting occurs simultaneously across the full bandwidth (0.9-2.45 μm) of the native spectrograph (final resolution varies linearly with wavenumber times largest delay). Y-axis is intensity, vertically offset for clarity.

Often for conventional radial velocimetry, instabilities in the EDI instrument lineshape is the critical limitation in achieving meter per second scale velocimetry precision.

In summary, the EDI method increases the resolution well beyond the classical limits enforced by the slit width and the detector pixel Nyquist limit and, in principle, decreases the effect of pupil variation on the instrument line-shape function. The EDI technique permits arbitrarily higher resolution measurements using the higher throughput, lower weight, size, fewer pixels, and smaller expense of a lower resolution spectrograph. The resolution boosting factor varies linearly with wavenumber and the maximum interferometer delay used, and there is no practical limit to the latter since it is typically in the few cm range for optical or NIR wavelengths. The resolution boosting occurs simultaneously across the whole bandwidth of the native spectrograph. Hence, one can use the boosting effect to produce a much wider bandwidth for a given spectral resolution at constant pixel number, or a much smaller pixel number for a given resolution and bandwidth. This is in contrast with a conventional dispersive spectrograph where the product of bandwidth and resolution is limited by pixel number.

1.2.1 EDI and Interferometric Spectral Reconstruction

The apparatus or technique we use for taking fringing data is called EDI, and EDI may also refer to the algorithmic use of the fringing data to measure a Doppler velocity shift, which was the original use of EDI. To distinguish what we are doing here, the algorithmic method for assembling a high resolution spectrum from EDI fringing data could be called interferometric spectral reconstruction (ISR), often abbreviated SR.

1.2.2 Compared to Fourier Transform Spectroscopy

Compared to a purely interferometric technique such as Fourier Transform Spectroscopy (FTS), ISR has a ∼30-100 times improved photon-limited signal to noise ratio (SNR) over the latter. (The photon S/N benefit compared to FTS goes as the square root of the number of native spectrograph resolution elements,[16] which is typically $\sim 10^4$ for an echelle spectrograph.) Since the ISR uses integrating time exposures– there is no continuously scanned delay– it is more robust to temporal fluctuations that can plague a FTS when observing a rapidly changing scene, such as spacecraft field-of-view sweeps. We have designed an EDI instrument that uses multiple delays in parallel which can make snapshot measurements of rapidly changing phenomena (see Figs. 12A & 12B of Ref. 4).

The ISR technique is mathematically related to another hybrid, dispersed-FTS,[17] but uses finer spectral channels and discrete fixed delays instead of scanning a single delay continuously over a range and reading out a time-dependent detector. All dispersed interferometer hybrids enjoy improved photon-limited S/N over undispersed interferometers.

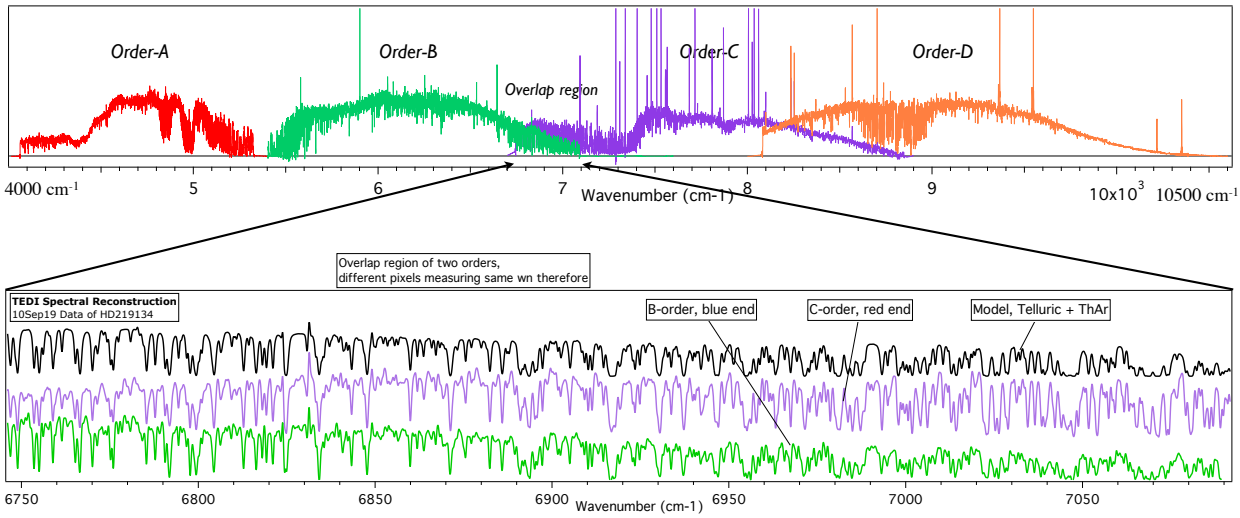

Figure 3. The TEDI reconstructed resolution boosted spectrum spans the 4 orders of TripleSpec spectrograph in NIR (4100-10500 cm^{-1}), here observing HD219134 on Sept 19, 2010. The lower graph is zoomed in region of overlapping orders B & C, showing agreement between two very unrelated groups of pixels (on opposite sides of detector), and with telluric model[14] (black curve).

Compared to an *internally* dispersed interferometer technique called Spatial Heterodyning Spectroscopy,[18] EDI has a much larger, essentially unlimited bandwidth, which does not require finely spaced pixels. The SHS has a much smaller bandwidth limited by the detector pixel spacing. The SHS produces a fringe comb which varies its periodicity rapidly with wavenumber. For features outside this bandwidth, the signal oscillates too finely to be resolved by the pixels.

2. RECONSTRUCTED SPECTRA

Observations of many stars were performed with the "TEDI" interferometer mounted within the central hole of the 200 inch primary mirror. Light from the interferometer was then dispersed by the TripleSpec[13] near-infrared echelle spectrograph. Continuous spectra between 950 and 2450 nm (4100-10500 cm^{-1}) with a resolution as high as ∼27,000 (10x boost), using 3 cm maximum delay, were recovered from data taken June 2011 with TripleSpec at a native resolution of ∼2,700. Figure 2 is an example of 10x resolution boosting. Figure 3 demonstrates the extremely wide bandwidth we can achieve, covering all four orders of the native spectrograph. Figures 5 & 6 shows closeups of the reddest order.

Data taken earlier than June 2011 have a smaller boost of 4x-6x (Figs. 3, 5, 6), since they were taken with contiguous delay up to only 2 cm maximum. We used eight delays, designated E1-E8, having values 0.1, 0.3, 0.7, 1, 1.3, 1.7, 3 and 4.6 cm, respectively. For this older data there was a gap in the delay coverage between E6 and E7 which prevented contiguous coverage of delay beyond 2 cm, even though E7 is 3 cm. This was remedied with the purchase of a 2.4 cm delay called E6.5 which we swapped with the E1 position in the 8-place rotary holder. (E1 is not essential, E2 can sense the lower frequencies).

3. WHAT'S NEW

3.1 Glass Dispersion Calibration Allows Wide Bandwidth Data Processing

Figure 3 shows the resolution boosted reconstructed spectra over 4 orders of the TripleSpec spectrograph, spanning 4100-10500 cm^{-1}. The wide bandwidth was processed more rapidly in the recent version of our code because we finished a careful calibration of the dispersion characteristics of all our glass etalons across the four orders we use (Fig. 4), by measuring the phase of a ThAr spectral lamp in the data and comparing to the theory based on known wavenumber[15] of each spectral line. Prior to having this calibration, and due to the many cycles of

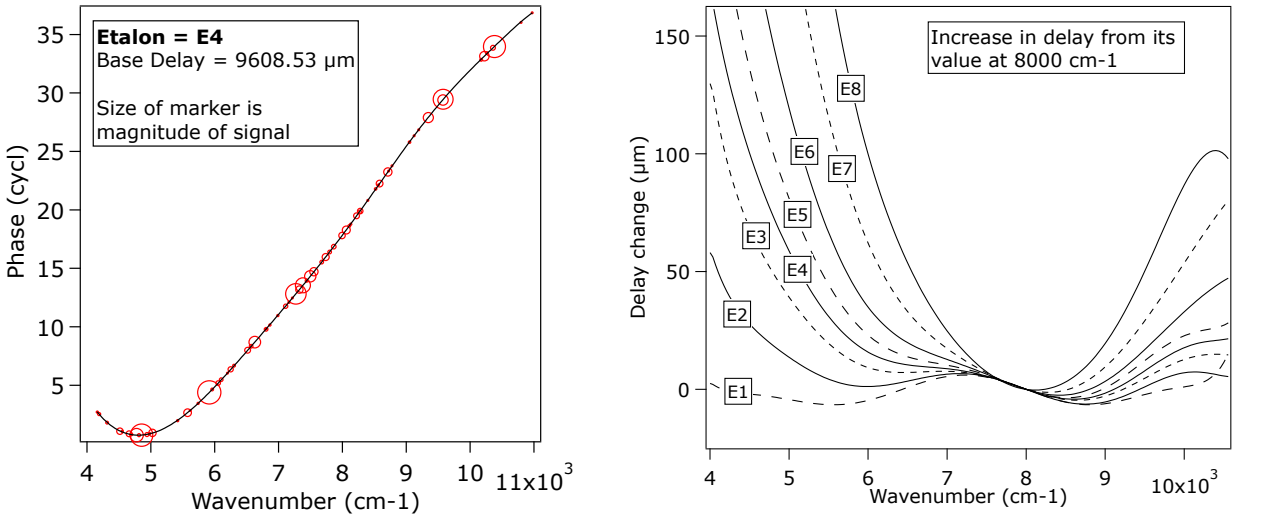

Figure 4. The dispersion characteristics of set of glass etalons are calibrated over a 4000-11000 cm^{-1} bandwidth by phase shift comparison with ThAr emission line model.[15] The resulting phase vs wavenumber curve (left), taken with a specific base delay value, is then used to "untwist" stellar fringing spectra so that a constant delay (the base value) can be used during reversal of heterodyning effect, in the processing prior to summing the individual channels to assemble the reconstructed spectra. The derivative of a 10th order polynomial fit to the phase data provides delay vs wavenumber curves (right). Only the phase curves, not the delay curves, are needed for the spectral reconstruction. But the family of delay curves are useful for detecting an integer fringe skip error in the phase shift measurement, by their common behavior. The dispersion characteristic of the beamsplitter substrate (most obvious in the smallest delay E1) is a common component of all. Delay values for E1-8 are $\sim$ 0.1, 0.3, 0.7, 1, 1.3, 1.7, 3 and 4.6 cm.

dispersive phase shift that can span an order for some large etalons, the data had to be processed piecemeal in small bandwidth chunks (fractions of an order) and phase manually adjusted for each etalon and each average wavenumber, which could be tedious. Now that the etalon dispersion is known, the current code computes the entire order at once and in principle could compute all orders at once.

The phase vs wn (left panel) is the only curve needed. It is applied directly to the fringing data (in complex spectra form) to remove the twist (linearly sloping phase vs wavenumber) due to glass dispersion. Without this "de-twisting", the periodic comb seen in some of the fringing data would not be perfectly periodic.

By taking the derivative of the phase vs wn, one creates a delay change vs wn curve (right panel). Although this is not needed for the de-twisting (the phase is the more immediately useful quantity), it is useful to plot the family of curves in order to recognize if one has made an integer fringe skip phase error, which is easy to do with the large etalons where the ThAr lines are sparse and the delay changes a large amount between those lines. Since they are made from the same type of glass, the family of curves should have the same shape after scaling by their physical length, and after subtracting away the unknown beamsplitter substrate contribution which is common to all the curves but is most prominent from the shape of the smallest etalon.

Once we have performed the de-twisting and removed the effects of glass dispersion, we can accurately recreate the shape of the continuum of the final spectrum by using the fringing information from the smaller etalons (see next subsection and Fig. 5[a]).

3.2 Continuum Shape from Fringing Data

In prior reports we produced composite output spectra that included the ordinary (nonfringing) spectrum to supply the majority of the lowest frequency information, that of the continuum and broadest features. The other source of these frequencies is the fringing information from the smallest delays, E1 and E2. The larger delays E3 through E8 supplied the higher frequency information. We had assumed that the ordinary spectrum would be more reliable and less noisy than the fringing derived component, especially since the ordinary was present in

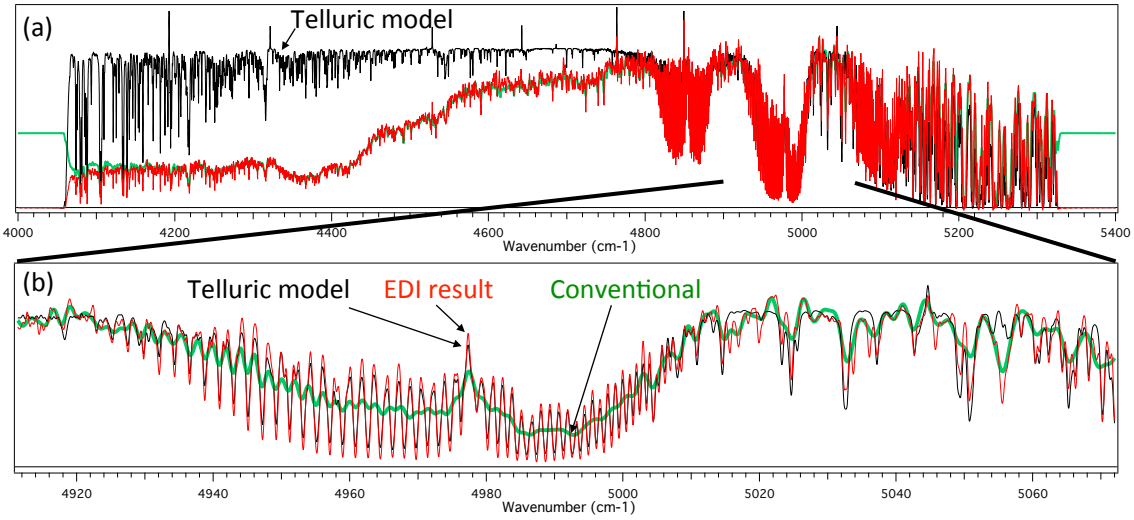

Figure 5. A-order spectral reconstruction (SR) results having 4x boost (11,000 resolution) for star HD219134+ThAr lamp, September 19, 2010. Black is telluric model, red is SR results, green is conventional (native, ordinary, nonfringing) spectrum. (a) full order 4100-5300 cm^{-1}. The shape of the continuum is accurately reproduced (comparing red to green curves) in spite of the signal coming from two very different kinds of components, fringing vs nonfringing. The red and green curves are lower than the black curve at the low wavenumber side because of coloration of TripleSpec disperser. (b) zoom in on a telluric feature near ∼4980 cm^{-1}due to CO_2 molecule.

each exposure for each etalon (delay) and thereby could be averaged over the 8 etalons. However, we discovered recently that we obtained cleaner results *omitting* the ordinary component (!) from the composite (Fig. 5, Fig. 6[c]). This indicates that the TEDI dataset is not photon limited but instrument limited. An important advantage of EDI is that it is extremely robust to fixed pattern errors that do not change synchronously with the dithering phase shifting. This could be, for example, a hot pixel that was not adequately suppressed during flatfielding.

Figure 5(a) shows excellent agreement in the shape of the continuum component, between the two methods of measuring it, ordinary (green curve) vs fringing data (red curve). This is made possible by the wide bandwidth calibration of the glass delay dispersion. Both the red and green curves show the same shape for the continuum portion, which deviates from the more constant continuum of the telluric model[14] (black curve) because of coloration of the TripleSpec disperser. Figure 6[c] compares the EDI result (red curve, "1x") using only fringing component blurred to 2700 to match the resolution of the native spectrograph, with the native spectrograph result (green curve). The EDI result agrees better with the details of the telluric model (black curve).

3.3 Improved Algorithm Fixes Ringing

A third recent accomplishment is improving the phase stepping algorithm so that the fringing output has very little nonfringing component in it (called leakage or pollution). This improves our SR output by eliminating a ringing artifact. This issue is described in section 4.1.1.

4. DATA PROCESSING

4.1 Phase Stepping Separates Fringing from Nonfringing

The purpose of phase stepping is to isolate the fringing component from the nonfringing by dithering the interferometer phase and seeking the component that follows the phase sinusoidally.

For each delay of the set E1-E8, the EDI takes phase stepped spectral data, which are a sequence of exposures where the interferometer phase is dithered over about one cycle. Figure 7 shows two example phase step exposures, zooming in on a single order (of four), for a small delay so that the interferometer comb acting on the

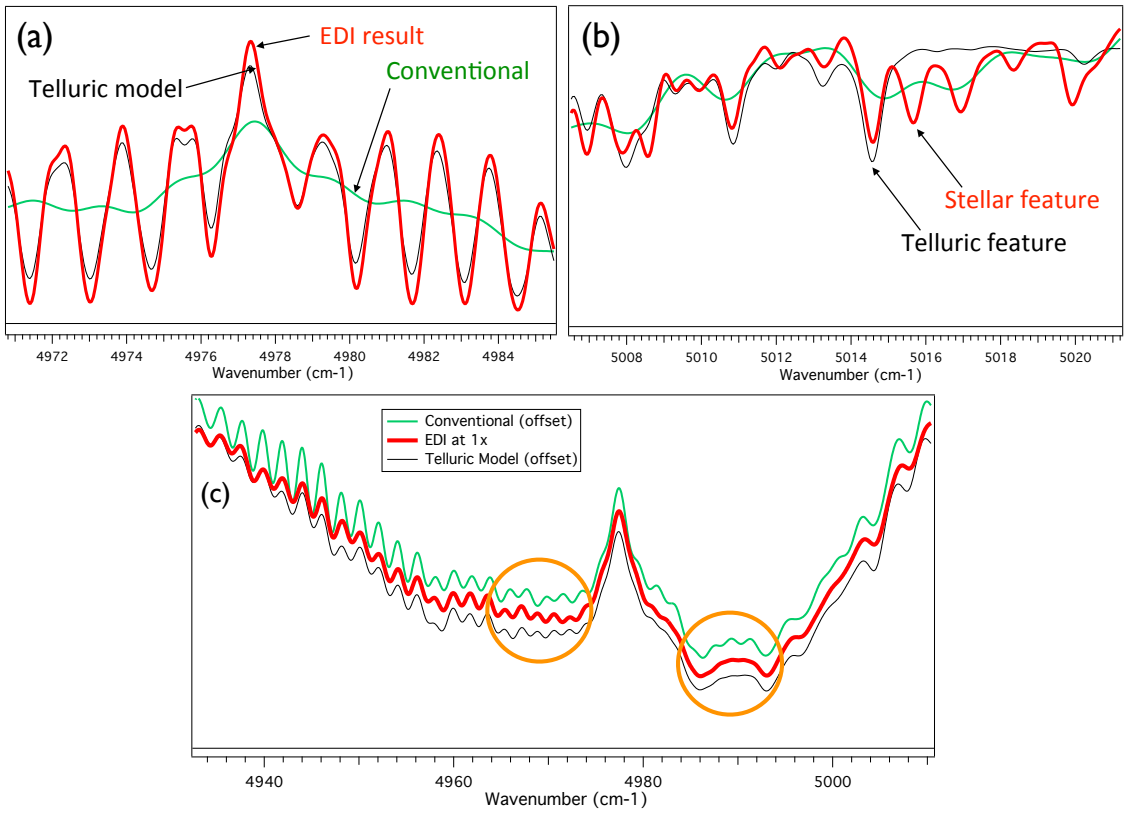

Figure 6. Zooms-ins of A-order SR result (bold red) of Fig. 5. (a) subtle features of telluric model (thin black), such as the tiny dips and detailed shapes of the peaks of CO_2 feature at ~4980 cm^{-1}, are beautifully reproduced. The ordinary spectrum (green) of native spectrograph cannot resolve these. (b) The current model does not yet contain stellar features, such as at 5016-18 cm^{-1}, because of individuality of each star's Doppler velocity, elemental constituents, photosphere temperature and pressure broadening. (c) The EDI result, ("1x") using only fringing measurements and blurred to have the same resolution (2700) as native spectrograph, more accurately follows the details of telluric model than the conventional spectrum obtained from same exposures. (See conventional's wiggles at 4970 & 4990 cm^{-1} disagreeing with model.) Green and black curves offset vertically for clarity ([c] only). Target is star HD219134+ThAr lamp, September 19, 2010

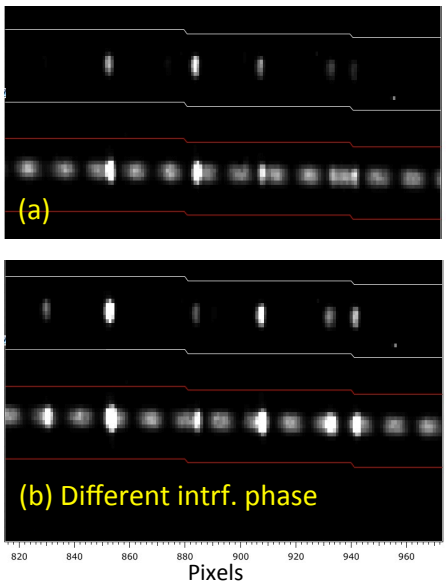

Figure 7. Effect of changing interferometer phase on a spectrum. Closeup of two raw exposures (a) & (b) having different interferometer phases, showing a single echelle diffraction order (of four used). Each order has four source fibers, A, B, and A_{sky} & B_{sky}. Thin pairs of white and red lines designate fiber A (white, top) or fiber B (red, lower). The adjacent sky fibers are not shown. Here, fiber A contains purely ThAr spectral lamp lines and fiber B a mixture of ThAr and stellar signals, but these roles are swapped in other exposures. Note that the phases of the ThAr lines, manifested by their modulated intensity, differ between exposures. The phase of the periodic stellar continuum also shifts by same amount, but it is perceived as a sideways translation rather than an intensity modulation.

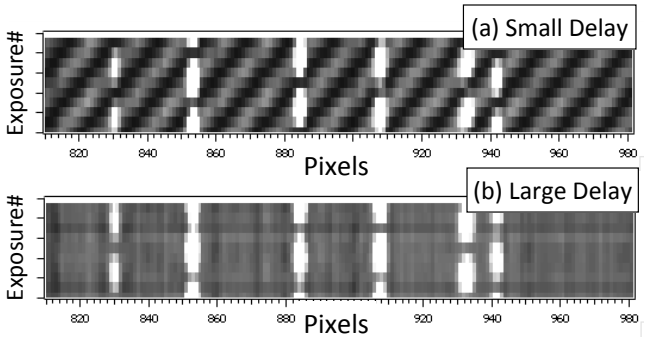

Figure 8. The format of input data to the phase stepping math is pseudo-multiphase, which is to stack the 10 individually recorded phase stepped 1D spectra into an array vs phase along the vertical, one for each of fiber sources, for four orders, for eight delays. This format of presentation for uniphase EDI data is similar to that of a single exposure of a multiphase EDI where phase varies along slit length. Examples of star+ThAr at two very different delays. Exposure # (phase step) on vertical axis; horizontal is X-pixel along dispersion direction. (a) Small delay (E1, 0.1 cm), the fringe comb period of starlight continuum is wide enough to be resolved. (b) Larger delay (E3, 0.7 cm), the starlight fringe comb is too fine to be resolved. However, since ThAr features are extremely narrow and isolated, they still manifest a fringe. Note their phase pattern is different between the two panels, and they constitute a "fingerprint" that can reveal the interferometer delay. Intensity fluctuations due to atmospheric seeing can be seen as horizontal features in bottom panel.

starlight continuum is resolved and easy to see. One sees the interferometer phase dither affecting the intensities of the ThAr lines, and the apparent horizontal shifting of the comb in the starlight. For each order, four 1d spectra are produced for each phase instance: fiber A sky, fiber A, fiber B, and fiber B sky. Of the two non-sky source fibers, A and B, one carriers starlight and the other a mixture of ThAr calibration lamp and starlight. The roles of A and B can be swapped during successive exposures.

The set of ten 1-d phase stepped spectra are stacked into an array (Figure 8) with phase in the Y-direction. These are the input to the phase stepping math. The stacking of 1d spectra produces a data format ("multi-phase") similar to the early type of EDI (see Fig. 5 of Ref. 1) which recorded in a single exposure phase that varied spatially along the spectrograph entrance slit by tilting of a interferometer mirror. However, because of the much wider bandwidth of TEDI relative to the earlier EDIs, the phase step interval along the Y axis, which is proportional to wavenumber, varies much more across each order (e.g.∼25%), which demands a more sophisticated phase stepping processing algorithm.

The purpose of the phase stepping math is to separate the fringing (Figure 9 bottom) and nonfringing (Figure 9 top) components from each other. Each 1d input spectrum contains a sum of fringing and nonfringing components. The fringing component can be distinguished because it is the only component that varies sinusoidally with phase. The data needs to be normalized to remove the fluctuation due to atmospheric seeing variation. Sometimes determining the correct amplitude of the ordinary component to normalize by is confused by the presence of the fringing portion.

We express the fringing component as a complex function vs pixel or wavenumber, called a whirl $\mathbf{W}(\nu)$, where the complex value manifests the phase and magnitude of the fringe (when in polar coordinates), or the cosine and sine amplitudes (when in rectangular coordinates). Rectangular coordinates is the preferred representation and required when performing the Fourier transform operations. The ordinary nonfringing spectrum is purely real and designated $B_{ord}(\nu)$. For a column of data of the multiphase input array (Figure 8) at a given wavenumber pixel ν_1, conceptually we fit a sinusoid plus an additive intensity offset to the data. The found intensity offset is assigned to $B_{ord}(\nu_1)$, and the found cosine and sine amplitudes are assigned to real and imaginary parts of $\mathbf{W}(\nu_1)$.

The precise values of the approximately known regular phase steps are found through iteration, which is especially rapid when processing the ThAr data. This produces a *delay* step

$$\Delta\tau_n = \lambda\Delta\phi_n/(2\pi) \tag{1}$$

that is *constant* for each exposure (row n of multiphase array) that describes the linearly changing phase vs wavenumber

$$\Delta\phi_n(\nu) = \nu\ 2\pi\Delta\tau_n \tag{2}$$

dependence across the whole band. In other words, although colloquially we frequently use the term "phase-stepping", it is actually *delay-* stepping that we describe. The $\Delta\tau$ is the dither on top of the bulk delay τ. Wavenumber $\nu = 1/\lambda$ is in units of cm^{-1} and is the natural unit for interferometry since for a constant delay (after glass dispersion removed) the sinusoidal combs are periodic in wavenumber, rather than in wavelength.

Using a forward model with preliminarily measured ThAr spectrum ($\mathbf{W}$, below), we find the $\Delta\tau$ which fits the 1d fringing spectrum for that particular exposure. Each ThAr line varies sinusoidally with $\Delta\tau$ and the fringe visibility is nearly ideal, so a precise $\Delta\tau$ is found promptly. Repeating for all 10 exposures, this yields delay step vs exposure #. Then applying Eq. 2 we find the phase steps for every X-pixel for every exposure. The phases found from the ThAr exposures are also applied to the stellar data measured simultaneously.

Our hardware commands the interferometer mirror to step with an average 0.25 μm for $\Delta\tau$. The measured values are typically uniform to within 0.01 μm or better. The algorithm does not require uniform steps but since we command uniform steps we use the measured degree of nonuniformity to alert us to problems in convergence of the iteration.

Rather than doing a sine fit to each individual column, it is equivalent and theoretically useful to construct the whirl and ordinary signals in a massively parallel method using the two equations below. For simplicity these are idealized to four exposures at 90° intervals, even though the actual phase steps differ from 90°, (especially

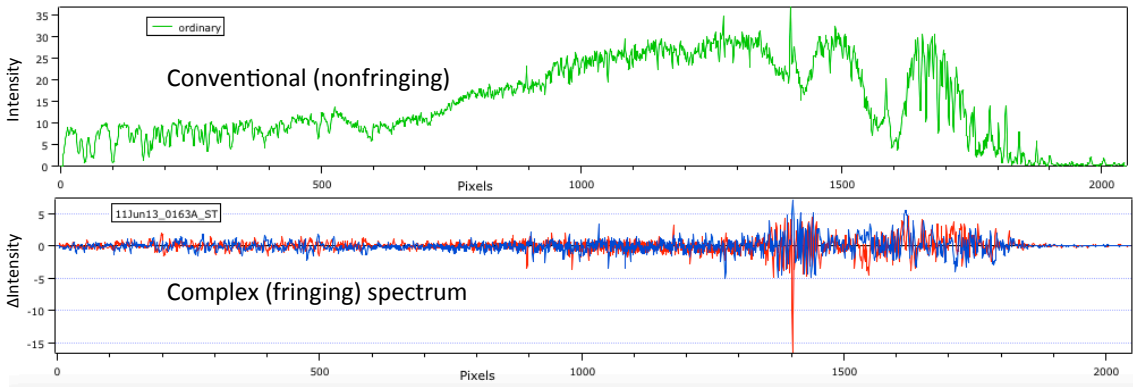

Figure 9. An ordinary (nonfringing) spectrum (a), and complex spectrum (fringing) called a "whirl" (b), are *both* produced from phase stepping math for each multiphase input array. Red and blue designate real and imaginary parts. Whirl magnitude is typically a few percent of ordinary spectrum. The target is star *11UMi plus weak ThAr lamp, and etalon E4 (delay ∼1 cm) is used. Vertical axis is intensity, in thousands of counts, and for bottom panel is change in intensity.

across a wide bandwidth, the phase steps vary while the delay steps are constant). The whirl and ordinary signals are

$$\mathbf{W} = \tfrac{1}{4}[(B_0 - B_{180}) + i(B_{90} - B_{270})] \ , \tag{3}$$

$$B_{ord} = \tfrac{1}{4}(B_0 + B_{180} + B_{90} + B_{270}) \ , \tag{4}$$

where B_n are the phase stepped 1D input data, with the wavenumber (ν) or pixel parameter suppressed for clarity but implied. These are sometimes referred to as "push-pull" equations. These are useful because the signal to noise properties are approximately the same as for the actual phase step case. For the actual phase step values, one can always find appropriate coefficients in these equations to satisfy the need in the first equation to cancel the fringes, and the need in the second equation to cancel the nonfringing component.

4.1.1 Algorithmic Improvements Prevent Leakage of Ordinary into Whirl

In early processing we noticed a ringing artifact that sometimes occurred in the SR output, which we sought to eliminate. Ringing can potentially occur for two reasons: (1) imperfect equalization so that the final modulation transfer function (MTF), [see section 4.4], is not perfectly Gaussian shape. For example from a gap in delay coverage, and a too high boosting factor such that the desired final Gaussian MTF stretches over the gap for which equalization cannot completely compensate. Let us call this "lineshape-ringing". (2) Leakage of some ordinary component in with the whirl output due to improper phase stepping math. Then when the whirl gets shifted in frequency during heterodyning reversal it also shifts the DC to some higher frequency where it does not belong, creating a ringing signal.

It is the latter that we are interested in discussing here. The ordinary signal contains a strong DC (zero frequency) component, whereas the fringing component is only a few percent in size. If the phase stepping algorithm is 99% perfect, it can still leave an undesired residual of ordinary component of ∼1% size, which is large enough compared to the few percent whirl to produce a significant ringing.

To isolate the source of the ringing problem to the second effect, we used an SR output (Fig. 5 and Fig. 10) with a conservatively low boosting of 4x (11,000 resolution) rather than the usual 6x. This ensured that there was no lineshape-ringing due to any gap in delay coverage. We inspected the very red end of the A-order where the telluric absorption is so high that we can be confident the true spectrum must go to zero in places, as suggested by the telluric model (Fig. 10). In prior processing we saw ringing in the regions, such as at 5208 cm^{-1}in panel (a).

We had noticed that the whirl for the ringing-plagued result had a broad pedestal having a similar shape as the ordinary spectrum, suggesting that the problem was that a few percent leakage of ordinary nonfringing component was polluting the whirl, (depicted in Fig. 10c). By forcibly subtracting a fraction of the ordinary to

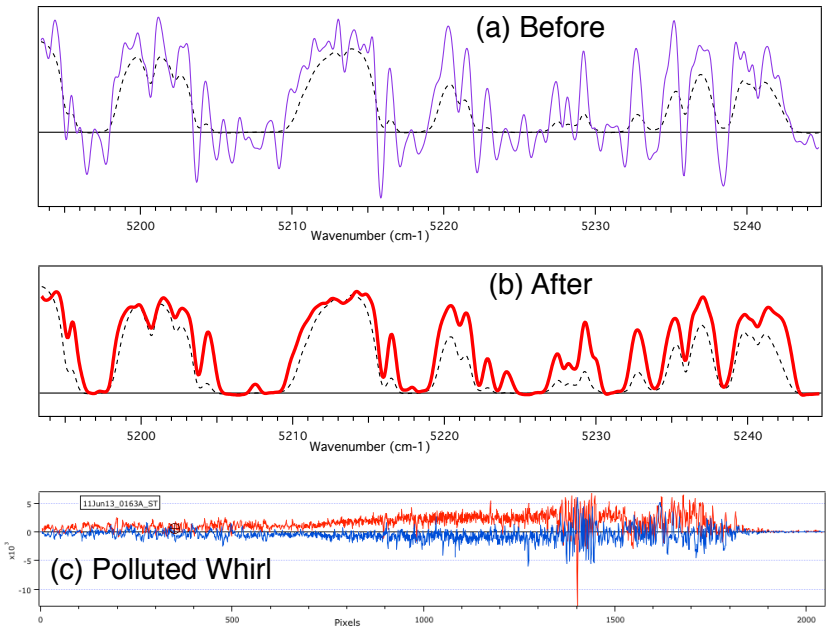

Figure 10. Ringing problem solved, by an algorithmic change in phase stepping math. (a) Earlier spectral reconstruction results had excessive ringing (thin purple), compared to telluric theory (dashed). An excellent place to explore this issue is in the deeply absorbing telluric region (such as ∼5200 cm^{-1}, shown here), since in spite of uncertain knowledge of telluric absorption depth, one can still be confident the measured spectrum must decrease to near zero in specific places where absorption is extremely high. (b) Ringing problem was solved by recognizing that a different normalization method for stellar data than for ThAr data was appropriate. Bad normalization for the stellar signal created "leakage" of ordinary into the whirl, which created a DC-like offset in the whirl (c), which when shifted in frequency during heterodyning reversal process became a ringing signal. Data on star HD219134.

produce a more ideal whirl, we confirmed this removed the ringing. Then we traced the source of the pollution to the particular method of computing the normalization amount. Changing the algorithm to another normalization method optimized for the stellar signal eliminated the pollution and the ringing issue, and we obtained the clean signal seen in panel (b).

4.2 Reversing the Heterodyning, Numerically

Figure 11 shows stages of heterodyning reversal processing, which numerically shifts the data in Fourier space to undo the heterodyning action applied optically by the interferometer. Figure 11(a) shows data of a small delay (E2, 0.34 cm) so that the spike of the continuum comb is apparent, but the same process is applied to each delay. For the larger delays there is no comb spike, or it is at such high frequency that it has wrapped to the opposite frequency branch (an effect called "aliasing"). The optical blurring of the spectrograph, which needs to be ∼2 to 3 pixels, prevents extreme aliasing of the very high delays.

A gentle lowpass filter is first applied to delete any aliasing artifacts near the Nyquist frequencies (±0.5 features per pixel). Then the data is shifted (left, in our case) by the amount set by the interferometer delay so that the comb spike, if it were present, would end up at zero frequency (b). Then the inverse Fourier transform is performed to bring the signal back to wavenumber space (d) and the imaginary part (which is usually small anyways if phasing is correct) is deleted. This forces the output spectrum to be a purely real spectrum, and is equivalent to adding the complex conjugate of the data to itself, which is similar to copying the left frequency branch to right branch and vice versa (c).

4.3 Assembling a Composite Spectrum from Many Delays

The heterodyning reversal is performed on each delay signal to form a set of spectra, one per delay. These have the appearance of wavelets at each isolated absorption or emission line. These are then summed to form a SR

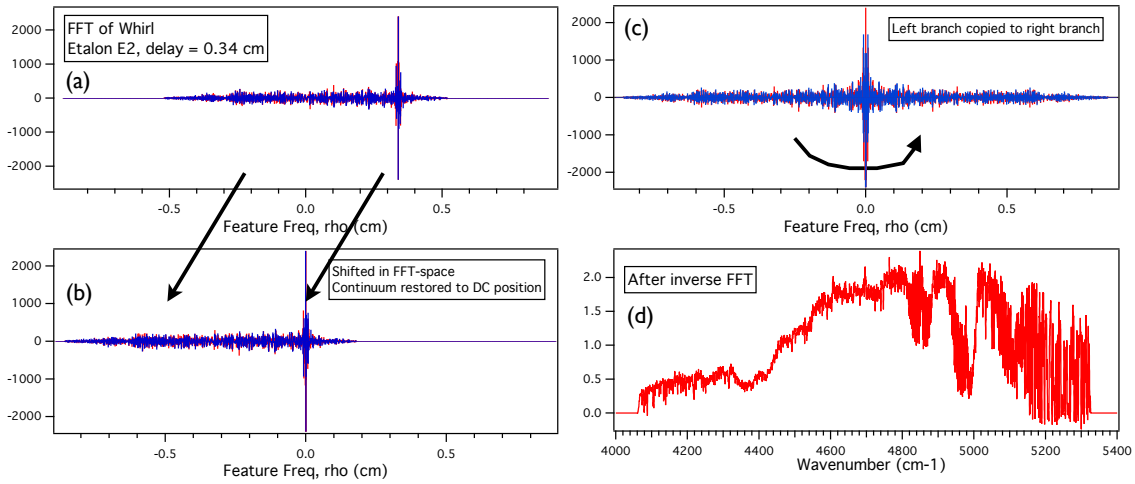

Figure 11. Stages of heterodyning reversal processing. (a) Fourier transform of whirl, here for etalon E2 having small delay of 0.34 cm. This puts continuum comb spike at 0.34 cm, which is within detectable range of native spectrograph ($-0.5 < \rho < 0.5$ cm^{-1}). Horizontal axis is frequency in features per cm^{-1}, having units of cm, same as delay space. Vertical axis limited to $\pm$2400, and spike actually is about $\pm$10,000 high. (b) The Fourier transform is shifted by the etalon delay, which moves the comb spike to zero frequency, along with moving other signal energy to left. For larger delay etalons there may be no comb spike and the signal energy ends up even further to the left. (d) The inverse Fourier transform is applied and the imaginary part set to zero to form a purely real output spectrum. This has same effect as (c) adding the complex conjugate to making the right and left frequency branches mirror reflections. Since the E1 and E2 etalons are small enough to produce a resolvable continuum comb, the resulting spectra will have all the information of an ordinary spectrum plus additional higher resolution information. By adding higher delay components, even higher resolution is produced in the composite final spectrum.

output, and the wavelets add to form narrow spikes.

Although we measure all eight delays E1-E8, we may only include in the compositing the lower subset of delays which cover delay space approximately contiguously, E1-E7. Also, our new protocol is to only use the fringing signals and not include the ordinary component. We find the ordinary component is not as clean as the E1 or E2 derived spectrum for measuring the lowest frequencies.

4.4 Equalizing the SR Output in Frequency Space

The SR output needs equalization as a final step, because if the delays are uniformly spaced then their conglomerate MTF shape will tend to be rectangular in shape rather than Gaussian. An overall Gaussian shape is desired to produce minimal ringing of the net instrument lineshape. Changing the shape of the MTF into an approximate Gaussian is the purpose of equalization.

The sensitivity of the EDI in frequency space, which is features per cm^{-1}, is called a Modulation Transfer function (MTF), which is also the Fourier Transform of the instrument lineshape. Figure 12 shows the net MTF for EDI is a shoulder to shoulder composite of peaks, one for each delay. This was measured by the ThAr data by comparison to the ThAr model. The ThAr MTF was assumed to also apply to the stellar signal measured simultaneously on the other fiber or the same fiber a few minutes later. The slightly nonuniform spacing of peaks composited together creates a lumpy MTF, and the lumpiness is undesirable.

The ideal MTF for general purpose spectroscopy is Gaussian shaped to avoid lineshape-ringing, and without gaps so every delay has good coverage. The lumpy shape of the MTF is removed by dividing by an inverse lumpy shape called the equalization. We get to choose the final resolution, that is, the breadth of this ideal Gaussian. Then the equalization is simply the ideal Gaussian divided by the ThAr data MTF. Then this equalization is applied to the stellar SR output.

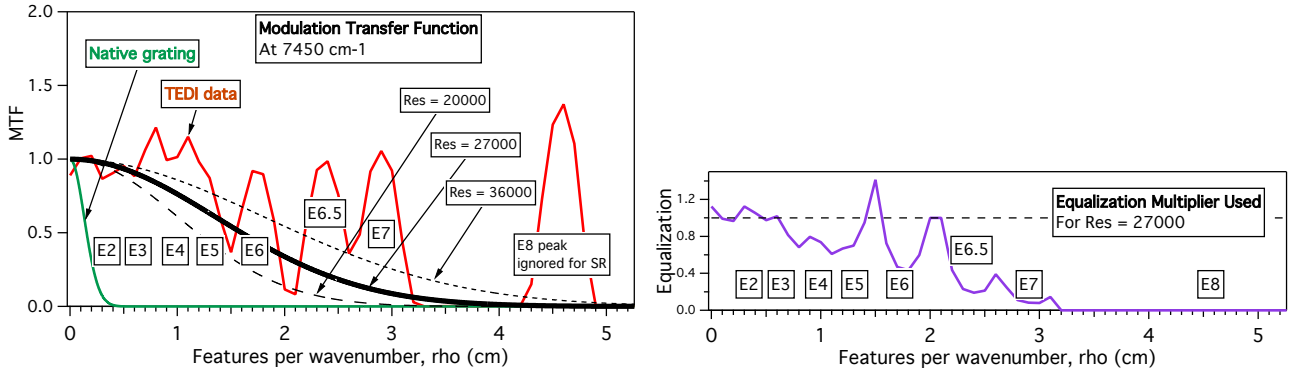

Figure 12. (Left) Net modulation transfer function (MTF) vs frequency ρ for several delays for the TEDI system near 7540 cm^{-1}(1.34 μm), for star κ_{CrB} on June 19, 2011. A MTF is the Fourier transform of the instrument lineshape, and the ratio of measured to theoretical frequency response. The magnitude of MTF is plotted as red curve. The spectrograph alone has the MTF of the thin green peak centered at the origin, whose width is proportional to its spectral resolution, in this case 2700. Including the TEDI interferometer creates a new peak having same width but centered at the interferometer delay. By using a series of delays which are contiguous, a composite MTF is formed (thick red curve) which covers the same wider ρ range as a higher resolution spectrograph. (Right) Equalization curve (purple) used to reshape MTF to approximate a Gaussian shape of res = 27,000 (thick black curve) shown in Fig. 2. By expanding the delay series (filling the gap between E7 & E8) we anticipate achieving resolution of 45,000 at 7500 cm^{-1}.

Since a wing of a Gaussian never truly reaches zero, but the data must eventually go to zero at some high frequency, some lineshape-ringing is inevitable. There is a tradeoff between increased resolution boost (which narrows the feature linewidth) and ringing amplitude outside the feature (which could obscure smaller neighboring features).

4.4.1 Gap in Delay Coverage Filled Using New Etalon E6.5

For the TEDI project, there is a significant gap in delay coverage between E7 and E8 (3.2 cm and 4.3 cm) which prevents increasing the boosting factor significantly beyond 10x, unless one is willing to tolerate larger lineshape-ringing. This is not due to any fundamental limitation of EDI, but the particular choice of etalon delays filling the 8 position rotary holder. These delay values were chosen to optimize Doppler velocimetry measurements, not ISR. Hence E8 was chosen to have a very high delay, not contiguous with the others, to be very sensitive to Doppler shifts for slowly rotating targets that would have narrow features of that frequency range.

For data taken prior to June 2011, which is most of the data, we also had a gap in coverage between E6 and E7 (2.0 to 2.7 cm). This gap limits the practical resolution boost to about 6x. Then beginning June 2011 we installed a new etalon called E6.5 whose delay of 2.4 cm sat between E6 and E7 but physically occupied the rotary wheel position previously occupied by E1. This allowed us to have an approximately contiguous delay coverage up to 3.2 cm, which allowed us to reach 10x boosting without significant lineshape-ringing.

5. NEW VISIBLE LIGHT EDI UNDER CONSTRUCTION

The ideal MTF for an EDI would have a more uniform coverage of delay space than in the TEDI project. We are building such an EDI, designed for spectral reconstruction in the visible band. The motivation is to provide high resolution and high accuracy lineshape stellar template spectra for use by other groups performing ~1 m/s precision Doppler radial velocimetry. These groups need high quality high resolution template spectra in order to accurately forward model the interaction between the stellar spectrum and the iodine absorption cell, which has many narrow features beyond the resolution limit of the native spectrograph. The 1 m/s velocity precision they desire is 10^4 times smaller than the typical stellar linewidth (usually set by stellar rotation), so accurate templates are required.

Figure 13 shows the optical layout for the new EDI, called "VEDI", under construction and planned to be used in series with the Lick Observatory Hamilton echelle. The 8 position rotary will be filled with etalons

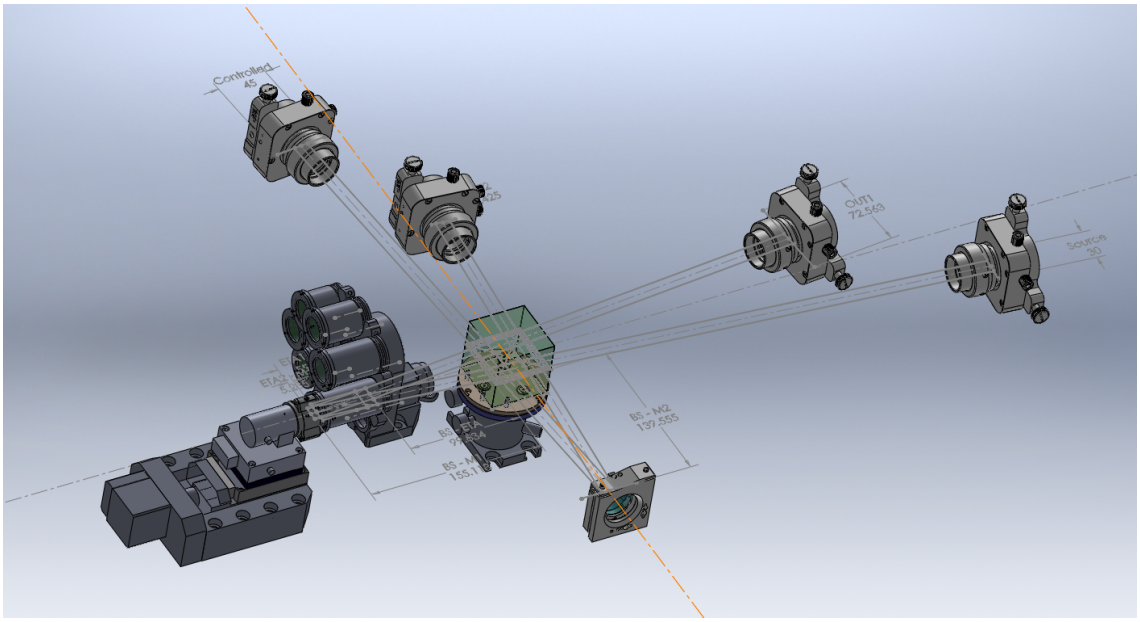

Figure 13. Optical layout for a new visible light EDI (VEDI) currently under construction and planned for use with the Lick Observatory's Hamilton echelle spectrograph to make high resolution stellar template spectra. The rotary holds eight choices of etalon length, which are in front of a mirror mounted on PZT/motorized translation stage. Scale of diagram is ∼0.7 m.

which provide a well-overlapped coverage of delay space. Fibers will conduct light to the interferometer from the spectrograph slit region and back, adapting to a pre-existing fiber scrambling unit used to study fiber stabilization of spectrograph PSF. Interferometer will be mounted inside the echelle room– potential heat sources such as calibration lamps will be located outside room via fiber.

5.0.2 EDI is Robust to Distortions That Affect Conventional Lineshape

For the conventional spectrograph, the highest feature frequencies are, *unfortunately*, measured by the extreme wing of the Gaussian-like MTF. Unfortunately, because the wing is where the MTF is not only the *least* sensitive, but it is most *vulnerable* to instrumental and environmental insults such as pupil changes, focal spot position and diameter drifts.

In contrast for the EDI, the heterodyning action shifts the native spectrograph MTF peak to a high frequency set by the delay. Thus the critically important high signal frequencies are measured at the central portion of the MTF, which is the most sensitive and stable portion. Numerical simulations (see Fig. 10 of Ref. 8) show that the sensitivity to many insults goes to zero at the very center of the MTF peak, such as a focal spot diameter and positional drift.

ACKNOWLEDGMENTS

This material is based upon work supported by the National Science Foundation under Grant No. AST-0505366, AST-096064, NASA Grant NNX09AB38G, and by Lawrence Livermore National Laboratory under Contract DE-AC52-07NA27344. Thanks to many contributions by Phil Muirhead, James Lloyd, Matt Muterspaugh, and Andrew Vanderburg. Thanks to Palomar Observatory and UC Berkeley Space Sciences staff including Mario Marckwordt, Michael Feuerstein, and Gregory Dalton.

REFERENCES

[1] Erskine, D. J., "An externally dispersed interferometer prototype for sensitive radial velocimetry: theory and demonstration on sunlight," *PASP* **115**, 255–269 (2003).

[2] Muirhead, P. S., Edelstein, J., Erskine, D. J., Wright, J. T., Muterspaugh, M. W., Covey, K. R., Wishnow, E. H., Hamren, K., Andelson, P., Kimber, D., Mercer, T., Halverson, S. P., Vanderburg, A., Mondo, D., Czeszumska, A., and Lloyd, J. P., "Precise stellar radial velocities of an M dwarf with a Michelson interferometer and a medium-resolution near-infrared spectrograph," *PASP* **123**(904), 709–724 (2011).

[3] Erskine, D. J. and Ge, J., "Novel Interferometer Spectrometer for Sensitive Stellar Radial Velocimetry," in [*Imaging the Universe in Three Dimensions: Astrphys. Advncd. Multi-Wavel. Imaging Devices*], van Breugel, W. and Bland-Hawthorn, J., eds., *ASP Conf. Series* **195**, 501–507 (2000).

[4] Erskine, D. J., "Combined dispersive/interference spectroscopy for producing a vector spectrum," *US Patent* **6,351,307** (Issued Feb. 26, 2002).

[5] Ge, J., van Eyken, J., Mahadevan, S., DeWitt, C., Kane, S. R., Cohen, R., Vanden Heuvel, A., Fleming, S. W., Guo, P., Henry, G. W., Schneider, D. P., Ramsey, L. W., Wittenmyer, R. A., Endl, M., Cochran, W. D., Ford, E. B., Martín, E. L., Israelian, G., Valenti, J., and Montes, D., "The first extrasolar planet discovered with a new-generation high-throughput Doppler instrument," *ApJ* **648**, 683–695 (2006).

[6] Edelstein, J., Muterspaugh, M. W., Erskine, D. J., Feuerstein, W. M., Marckwordt, M., Wishnow, E., Lloyd, J. P., Herter, T., Muirhead, P., Gull, G. E., Henderson, C., and Parshley, S. C., "TEDI: the TripleSpec Exoplanet Discovery Instrument," *Proc. SPIE* **6693** (2007).

[7] Mahadevan, S., Ge, J., Fleming, S. W., Wan, X., DeWitt, C., van Eyken, J. C., and McDavitt, D., "An inexpensive field-widened monolithic michelson interferometer for precision radial velocity measurements," *PASP* **120**, 1001–1015 (2008).

[8] Erskine, D. J. and Edelstein, J., "High-resolution Broadband Spectral Interferometry," *Proc. SPIE* **4854**, 158–169 (2003).

[9] Erskine, D. J., Edelstein, J., Feuerstein, M., and Welsh, B., "High resolution broadband spectroscopy using an externally dispersed interferometer," *ApJ* **592**, L103–L106 (2003).

[10] Erskine, D. J. and Edelstein, J., "Interferometric resolution boosting for spectrographs," *Proc. SPIE* **5492**, 190–199 (2004).

[11] Erskine, D. J., Edelstein, J., Muirhead, P., Muterspaugh, M., Covey, K., Mondo, D., Vanderburg, A., Andelson, P., Kimber, D., Sirk, M., and Lloyd, J., "Ten-fold spectral resolution boosting using TEDI at the Mt. Palomar NIR Triplespec spectrograph," *Proc. SPIE* **8146** (2011).

[12] Edelstein, J., Erskine, D. J., Sirk, M., Vanderburg, A., and Wishnow, E. H., "Enhanced spectral resolution via externally dispersed interferometry," *Proc. SPIE* **8446** (2012).

[13] Wilson, J. C., Henderson, C. P., Herter, T. L., Matthews, K., Skrutskie, M. F., Adams, J. D., Moon, D.-S., Smith, R., Gautier, N., Ressler, M., Soifer, B. T., Lin, S., Howard, J., LaMarr, J., Stolberg, T. M., and Zink, J., "Mass producing an efficient NIR spectrograph," *Proc. SPIE* **5492**, 1295–1305 (2004).

[14] Roe, H. G., *Titan's atmosphere at high-resolution*, PhD thesis, Univ. California, Berkeley (2002).

[15] Kerber, F., Nave, G., and Sansonetti, C. J., "The Spectrum of Th-Ar Hollow Cathode Lamps in the 691-5804 nm region: Establishing Wavelength Standards for the Calibration of Infrared Spectrographs," *ApJS* **178**, 374–381 (2008).

[16] Beer, R., [*Remote Sensing by Fourier Transform Spectrometry*], John Wiley, New York (1992).

[17] Behr, B. B., Hajian, A. R., Cenko, A. T., Murison, M., McMillan, R. S., Hindsley, R., and Meade, J., "Stellar astrophysics with a dispersed Fourier transform spectrograph. I. Instrument description and orbits of single-lined spectroscopic binaries," *ApJ* **705**, 543–553 (2009).

[18] Harlander, J., Reynolds, R., and Roesler, F., "Spatial Heterodyne Spectroscopy for the Exploration of Diffuse Interstellar Emission Lines at Far-ultraviolet Wavelengths," *ApJ* **396**, 730 (1992).